EUROFUSION WPMST1-CP(16) 15153

D Carralero et al.

Recent progress towards a functional model for filamentary SOL transport

Preprint of Paper to be submitted for publication in
Proceedings of 26th IAEA Fusion Energy Conference

This work has been carried out within the framework of the EUROfusion Consortium and has received funding from the Euratom research and training programme 2014-2018 under grant agreement No 633053. The views and opinions expressed herein do not necessarily reflect those of the European Commission.

Recent progress towards a quantitative description of filamentary SOL transport

D. Carralero[1], H. W. Müller[1,2], M. Groth[3] M. Komm[4], J. Adamek[4], L. Aho-Mantila[5], S. A. Artene[1,6], G. Birkenmeier[1,6], M. Brix[7], G. Fuchert[1,9], P. Manz[1,6], J. Madsen[8], S. Marsen[7,9], U. Stroth[1], H. J. Sun[1], N. Vianello[10,11], M. Wischmeier[1], E. Wolfrum[1], ASDEX Upgrade Team[1], COMPASS Team[4], JET Contributors[12] and the EUROfusion MST team[13].

[1]Max-Planck-Institut für Plasmaphysik, Garching, Germany. [2]Institute of Materials Chemistry and Research, University of Vienna, Währingerstrasse 42, A-1090 Vienna, Austria. [3]VTT Technical Research Center of Finland, Helsinki, Finland. .[4] Institute of Plasma Physics AS CR, Prague, Czech Republic. [5]Aalto University, Espoo, Finland. [6]Physik-Department E28, Technische Universität München, Garching, Germany. [7]EUROfusion Consortium, JET, Culham Science Centre, Abingdon, OX14 3DB, UK, [8]The Technical University of Denmark, Department of Physics, DK-2800 Kgs. Lyngby, Denmark, [9]Max-Planck-Institut für Plasmaphysik, Greifswald, Germany. [10]Consorzio RFX, Associazione Euratom-ENEA sulla fusione, C.so Stati Uniti 4,I-35127 Padova, Italy. [11]Ecole Polytechnique Fédérale de Lausanne, Centre de Recherches en Physique des Plasmas, Lausanne, Switzerland. [12]See the Appendix of F. Romanelli et al., 25th IAEA Fusion Energy Conference 2014, Saint Petersburg, Russia. [13]See http://www.euro-fusionscipub.org/mst1.

E-mail contact of main author: daniel.carralero@ipp.mpg.de

Abstract. A summary of recent experiments on filamentary transport is presented: L-mode density shoulder formation is explained as the result of a transition between sheath limited and inertial filamentary regime. Divertor collisionality is found to be the parameter triggering the transition. A clear reduction of the ion temperature takes place in the far SOL after the transition. This mechanism seems to be generally applicable to inter-ELM H-mode plasmas, although some refinement is still required.

1. Introduction

Heat and particle transport onto plasma-facing components of fusion devices is determined in the Scrape-off Layer (SOL) by the balance between parallel and perpendicular transport. While parallel transport is mostly caused by conduction, perpendicular transport can have a dominant contribution due to perpendicular convection of coherent structures known as filaments. This is a key issue for next generation tokamaks, as the filaments will determine the erosion levels and the heat loads at the main chamber first wall.

Basic models for filaments [1] describe their ExB propagation as the result of a polarization caused by curvature drifts [2]. In order to keep charge conservation, conventional models had this polarization compensated by a parallel current flowing along the filament into the wall [3]. This is known as the Sheath Limited regime (SL). It was later proposed that some mechanisms, such as a large increase of SOL collisionality, might electrically disconnect the midplane from the walls, leading to the so-called inertial regime (IN). The transition from SL to IN regime could have important global implications, as it would cause filaments to propagate faster [3,4] and lead to an enhanced perpendicular transport [5], thus potentially increasing particle and heat loads on the first wall. A well known example of this would be the onset of the density profile flattening known in the literature as the density “shoulder”, reported in many tokamaks when a certain density threshold is exceeded during L-mode operation [6-8], and which has been explained as the result of filament disconnection from the wall [9].

Previous work carried out on ASDEX Upgrade (AUG) [10] already established the relation between shoulder formation and a clear transition in the properties of filaments. The threshold coincided with the point where collisions disconnected the midplane from the wall. Such a disconnection was defined using the effective collisionality criterion proposed by Myra et al. [11], $\Lambda > 1$, where $\Lambda = \frac{L/c_s}{1/\nu_{ei}} \frac{\Omega_i}{\Omega_e}$, and L is the parallel scale length, c_s the sound speed, ν_{ei} the electron–ion collision frequency and Ω_α the gyrofrequency of species α. Later work confirmed these results in a multimachine study including the tokamaks JET, AUG and COMPASS[13], which due to their similar magnetic configuration and difference in size form a "Stepladder" to ITER [12]: In the first two, the density was high enough to achieve $\Lambda > 1$, and both the filament transition and the shoulder formation were observed. In COMPASS, where $\Lambda > 1$ was not achieved, filaments and density profiles remained constant for the whole range of observed densities. Still, it could not be decided if the process was triggered by the density – as suggested by previous literature -, the collisionality in the midplane, Λ_{mid} (defined using far SOL T_e and n_e values and the connection length as L), or the local collisionality at the divertor, Λ_{div} (defined using T_e and n_e at the divertor target and a fraction of the connection length as L).

In this work, we present the experimental effort that has been carried out in recent years in the subject of understanding the basic mechanism determining filamentary transport in order to improve current estimations of first wall loads for ITER and DEMO. Most of this work has been done in L-mode plasmas, which allow for greater diagnostic coverage. However, the conclusions achieved in such simplified L-mode experiments are later expanded into the more relevant H-mode. In section 2, the parameter triggering the transition is determined. In section 3, a study on the scaling of filaments is presented. In section 4, the impact on SOL temperatures is discussed. Finally, previous results are extended to H-mode in section 5 and conclusions are outlined in section 6.

2. The role of divertor collisionality

In order to disentangle the relative contributions of midplane and divertor collisionalities in the shoulder formation, a series of L-mode density ramps were carried out on AUG [14]. Different heating powers (including pure ohmic, 300 and 600 kW of ECH power) were used. Also, some 300 kW discharges using nitrogen seeding were included in the analysis (although no filament data is available in these). Density profiles were measured using a lithium beam [15], and filaments in the far SOL ($\rho_p \sim 1.02$) were characterized using a multipin Langmuir probe mounted on a midplane manipulator (MPM) [10]. Also, divertor density and temperature were measured by flushed mounted Langmuir pins at the target plates. As can be seen in Fig. 1a, the T_e drop at the divertor associated to the high recycling regime of the LFS divertor takes place at different densities (indicated here as the line integrated density at the edge, $n_{edge,}$ measured by interferometry) depending on power and seeding. This results, as seen in Fig. 1b, in $\Lambda_{div} > 1$ being achieved at different n_{edge} values. Instead, as will be seen in Section 4, T_e in the far SOL does not depend on the heating power, and Λ_{mid} remains constant practically for the whole range of n_{edge}. In Figs. 1c and 1d, it is clear that the transition does not take place for a given density value, as filament size, δ_b, and the density e-folding length in the far SOL, λ_n, increase at different n_{edge} values. Λ_{mid} is neither the driving parameter, as it remains constant through the transition in all cases. Instead, as shown in Fig. 1e and 1f, all points converge into a single curve when δ_b and λ_n are represented as a function

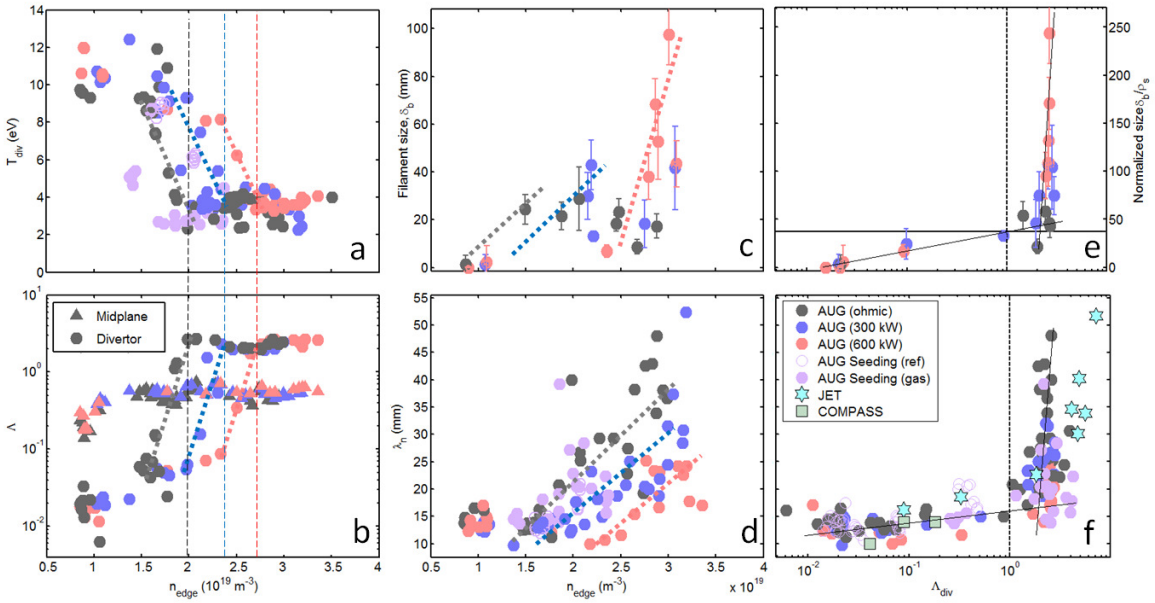

FIG. 1. L-mode shoulder formation experiments. Color indicates heating power and seeding. Circles/stars/squares indicate data from AUG/JET/COMPASS; a) Evolution of divertor T_e with plasma density b) Collisionality at the divertor/midplane (circles/triangles) as a function of density. Vertical dashed lines indicate the onset of detachment at the LFS divertor; c) and d) Evolution of filament size and λ_n as a function of edge density; e) and f) Evolution of filament size and λ_n as a function of divertor collisionality.

of Λ_{div} regardless of heating power or seeding. In this case, two clear regimes can be seen, with global particle transport becoming strongly enhanced for $\Lambda_{div} > 1$. Interestingly, seeded discharges (represented in Fig. 1 as hollow/solid violet circles indicating the times in the discharge before/after the seeing) converge with the others, indicating that the result is independent from how the high collisionality is achieved. In Fig. 1f data points from JET and COMPASS have also been included, in good agreement with previous results [12]: In JET, where $\Lambda_{div} > 1$ values are achieved, a transition remarkably similar to the one at AUG is observed. In COMPASS, where $\Lambda_{div} < 1$ for the whole data set due to a more limited range of achievable densities, all data points are in the low collisionality branch of the figure.

3. A change of filament scaling

As explained in the Introduction, a transition between SL and IN filamentary regimes has been proposed as the explanation for the shoulder formation [9]. This would be consistent with the strong change of scaling of filament size shown in Fig. 1e, which clearly mirrors that of λ_n. Nevertheless, this transition has been observed in basic plasmas [16] but was yet to be confirmed in fusion-relevant machines like AUG. Therefore, in order to verify this hypothesis, the scaling of filament size as a function of perpendicular velocity was studied in the experiments described in the previous section [14]. Sheath limited filaments scale as $\delta_b \propto (v_{perp})^{-2}$ [3], while filaments in the inertial regime scale as $\delta_b \propto (v_{perp})^{1/2}$ [3]. By using a multipin probe head to calculate correlations between radially and poloidally spaced pins, the sizes and perpendicular velocities of conditionally averaged filaments during the density ramps were obtained [10]. As can be seen in Fig. 2, a clear transition in the scaling is observed around $\Lambda_{div} = 1$, with filaments in the $\Lambda_{div} < 1$ branch scaling according to the SL model, and filaments in the $\Lambda_{div} > 1$ branch according to the IN. The transition is indicated in the figure by a vertical solid line which corresponds to the size for which the collisionality

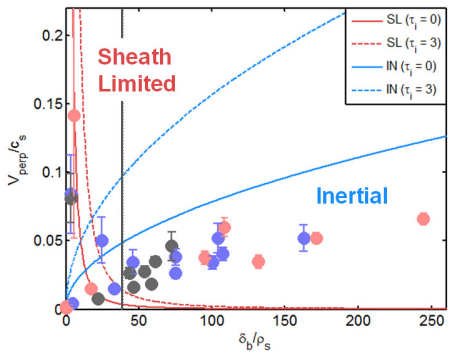

FIG. 2. L-mode filament regime transition [14]. Filament perpendicular velocity is represented as function of perpendicular size (circles. Same color code as in Fig 1). Inertial and Sheath limited scalings are presented as a reference. The black vertical line corresponds to the level indicated in Fig 1e) by the horizontal black solid line

threshold is achieved in Fig. 1e, where it is marked as a horizontal solid line. In order to illustrate this, theoretical predictions [17] for both regimes have been also represented in the figure considering both cold and warm ions, with $\tau_i = T_i/T_e$. Interestingly, IN regime filaments are clearly better modelled by the cold ion approximation. This novel result confirms that, coinciding with the onset of the density shoulder, the disconnection of filaments caused by a critical collisionality value leads to a transition of the propagation mechanism of filaments, which become larger and denser.

4. Effect of the shoulder formation on SOL temperatures

The evolution of T_e and T_i through the onset of the density shoulder has been investigated, as it determines the amount of energy transported by filaments and background. First, T_e was measured by means of a swept Langmuir pin installed on the MPM. By plunging the probe close to the separatrix at high and low Λ_{div} conditions, a typical radial profile can be obtained for each case. As can be seen in Fig. 3, both profiles are quite similar in the far SOL were T_e remains roughly constant at T_e ~ 10-15 eV. This is consistent with previous measurements in AUG [18]. Instead, a drop in T_e is observed in the near SOL at high collisionality. This can be explained as the result of the general cooling of the plasma when the density is increased to achieve high Λ_{div} while the heating power is kept constant. T_e was also measured at ρ_p ~ 1.02 during the density ramps discussed in previous sections. As can be seen in the insert of Fig. 3a, with the only exception of very low densities (corresponding to collisionality values of Λ_{div} ~ 0.01), a constant T_e ~ 15 eV is observed regardless of heating power or n_{edge}.

Second, T_i has been measured in the far SOL by means of a Retarding Field Analyzer (RFA) installed on the MPM [19]. In this case, discharges with different constant density levels were carried out on AUG featuring low and high collisionalities (Λ_{div} ~ 0.01and Λ_{div} ~10). In each case, the MPM was plunged to different distances to the separatrix to form a radial profile in the far SOL. Unfortunately, in this case no measurements are available close to the near SOL. By conditional averaging, T_i values of filaments and background are calculated separately. As can be seen in Fig. 3b, a strong reduction of T_i takes place after the transition: for Λ_{div} ~ 0.01, a radial exponential decay can be seen both for filaments and background, while for Λ_{div} ~10 the profile seems to remain radially constant at T_i ~ 20 eV for both. This result is in good agreement with the fact that disconnected filaments fit better with the cold IN regime, as discussed in Fig. 2. In this case, a drop in separatrix T_i can not be accounted for this change, as it goes from $T_{i,sep}$ ~ 175 eV to $T_{i,sep}$ ~ 150 eV over the transition, as measured by CXRS. Also, as can be seen in theinsert of Fig. 3b, before the transition, filaments are clearly

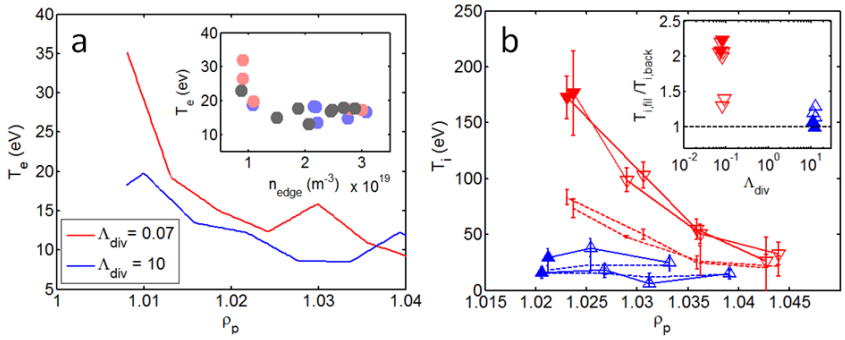

FIG. 3. L-mode temperature measurements. Red/blue color indicates low/high collisionality; a) Radial profiles of T_e , as measured by the Langmuir probe. On the insert, T_e measurements at ρ_p ~ 1.02 during several density ramps. Color code as in Fig. 1; b) Radial profiles of T_i. Solid/dashed lines stand for filaments/background. On the insert, the ratio of the filament to background T_i is displayed. Solid symbols stand for the innermost radial positions.

warmer than the background at the innermost positions, while similar values are measured for high Λ_{div}. Interestingly, filament T_i value, which seems to increase exponentially as the separatrix is approached, is already similar to $T_{i,sep}$ at ρ_p ~ 1.02, suggesting that these structures must be generated inside the confined plasma, where T_i is equal or greater than the one measured in the filament at the far SOL.

5. H-mode shoulder formation

Since next generation machines will be with all likelihood operated in H-mode, any attempt to predict their behavior must be valid in this regime of confinement. Therefore, an additional line of work was dedicated to determine the validity of the L-mode studies in H-mode [20]. With this aim, a series of discharges have been carried out in AUG in which the L-mode scenario with 300 kW of heating power used in previous work was achieved as a reference, and then brought into H-mode by increasing the heating power up to 1-4 MW. Then, the collisionality in the divertor was increased by increased fueling or nitrogen seeding, in order to reach the $\Lambda_{div} > 1$ condition. In order to disentangle the effects of nitrogen and deuterium fueling on the Λ_{div} values, different fueling rates for both gases (N_{rate} and D_{rate}) were used, roughly dividing the data set in four scenarios, as detailed in Table 1: A) low power discharges with low N_{rate} and D_{rate} values; B) discharges including both NBI and ECH heating, strong nitrogen seeding and a low D_{rate}; C) A discharge in which $\Lambda_{div} > 1$ is achieved only by means of a strong density fueling with no nitrogen; D) discharges with full power, and both high N_{rate} and D_{rate} values. As before, density e-folding length, λ_n, and filament size, δ_b, were measured with the LiB and MPM diagnostics, respectively. Thermoelectric currents to the divertor [21], I_{div}, are used to detect ELMs in order to separate conditionally averaged inter-ELM values of all measurements [20].

Results are presented in Fig. 4 following the same arrangement employed in Fig. 1 for L-mode results: First, in Fig. 4a and c, δ_b is presented as a function of n_{edge} and Λ_{div}, respectively. As can be seen, a filament transition takes place for L-mode filaments at n_{edge} ~ $2 \cdot 10^{19}$ m^{-3}, which coincides with the value for the 300 kW discharges in Fig 1. Then, when additional power is injected to access H-mode, the collisionality is reduced again and δ_b drops. Finally, when density is increased over a second threshold, n_{edge} ~ $3.5 \cdot 10^{19}$ m^{-3}, a similar transition takes place for H-mode inter-ELM filaments. As in Fig. 1e, both transitions converge and take place around Λ_{div} ~ 1 when represented as a function of collisionality.

Shot	Scenario	P_{ECH} (MW)	P_{NBI} (MW)	$D_{rate\ t=3.5\ s}$ (10^{21} s^{-1})	$N_{rate\ t=4.5\ s}$ (10^{21} s^{-1})	D_{rate} max (10^{21} s^{-1})	N_{rate} max (10^{21} s^{-1})	$T_{e,div}$ min (eV)
31974 (○)	A) Low N, Low D	1.3	-	1.3	2.8	1.3	3.4	1
31977 (□)		1.9	-	1.3	2.8	1.3	3.8	0
33055 (○)	B) High N, Low D	1.3	1.7	6	1.8	6	8	1.5
33057 (□)		1.3	1.7	8.2	1.8	8.2	8	3
33056 (○)	C) High D, no N	1.3	1.7	6.3	-	24.5	-	10
33058 (○)	D) High D, High N	1.3	1.7	6.3	2	15.4	8	5
33059 (□)		1.3	1.7	6.3	4	24	4	5
33475 (◊)		1.4	1.7	6.2	5	24.4	5	7.5
33478 (Δ)		1.4	2.4	7	9.2	24.4	9.2	1.5

Table 1. Main parameters of the H-mode experiments [20]. The four scenarios A-D are grouped in four colors (respectively, blue/green/black/red), based on their D_{rate}, N_{rate} values.

Regarding the onset of the shoulder, represented in Fig. 4b and d, the same general trend as in L-mode is observed when considering the point cluster as a whole: Shoulder formation coincides again with both the $n_{edge} \sim 3.5 \cdot 10^{19}$ m^{-3} threshold for H-mode filament transition and with the general $\Lambda_{div} \sim 1$ transition condition, with points taking similar values as the ones in Fig. 1f (indicated in Fig. 4d as a shaded area). However, when the four scenarios are considered individually, a clearer trend is found: discharges from scenario A display low levels of Λ_{div} and do not access the higher transport regime. The same is valid essentially for scenario C, albeit slightly higher Λ_{div} (and thus λ_n) values are achieved. Instead, all discharges from scenario D develop a clear shoulder, achieving a significant increase in λ_n at higher values of Λ_{div}. Interestingly, discharges in scenario B, displaying similar Λ_{div} and n_{edge} values as those in scenario D, fail to achieve high λ_n values. This reveals a more complex picture than in L-mode, as $\Lambda_{div} > 1$ seems to be necessary but not sufficient for the shoulder formation, with the level of D_{rate} playing also some role in it. Since scenarios B and D feature similar n_{edge} values, such a role is not likely to be related to the fueling of the main plasma, but instead to some mechanism taking place in the SOL. Thes result is consistent with L-mode observations carried out in TCV, where also a minimum level of fueling has been found to play a role in shoulder formation [22]. One possible explanation for this would be that the shoulder formation requires a high recycling rate at the main wall on top of the increased convective transport [23]. This would be consistent with the ion cooling described in the previous section. Nevertheless, the precise determination of this second threshold and the identification of the underlying physical mechanism will be the subject of forthcoming work.

6. Conclusions

Experiments carried out in AUG show how divertor collisionality, Λ_{div}, is the parameter triggering the shoulder formation in L-mode plasmas. Also, a change in filamentary regime has been measured for the first time in a fusion-relevant machine, linking the transition associated to filament disconnection from the wall to the formation of the density shoulder. These results lead to a scaling of λ_n which is common for the three tokamaks of the "ITER Stepladder": COMPASS, AUG and JET. Further experiments carried out in AUG show that the formation of the L-mode shoulder is also characterized by a strong cooling of the far SOL, which brings T_i of both filaments and background to levels similar to those of T_e, $T_e \approx T_i \approx$ 15-20 eV. An attempt has been carried out to extend these results into H-mode: First, the formation of a shoulder has been confirmed in inter-ELM H-mode plasmas. Second, the link

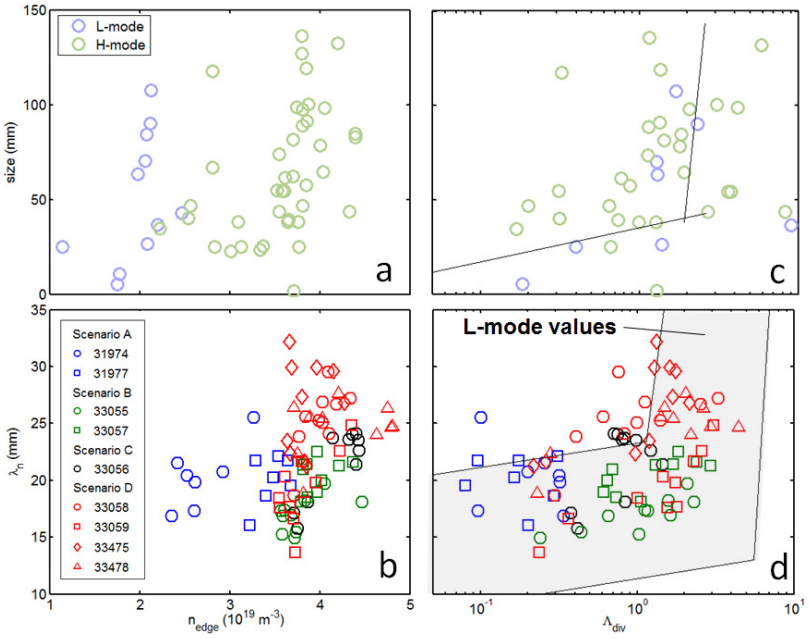

FIG. 4. H-mode shoulder formation experiments [20]; Size of filaments as a function of a) density and c) collisionality. Blue/Green colors stand for L/H-mode. Solid lines in c) correspond to the L-mode scaling shown in Fig. 1e); b) and d) show respectively the e-folding length as a function of density and collisionality. Color stands for the experimental scenario. Shaded area in d) represents the range of L-mode values shown in Fig. 1f).

between shoulder formation and filament transition has also been found to remain generally valid: Collisionality remains the necessary condition for the shoulder formation, but deuterium fueling seems to play an additional role. These results allow the extension of the general shoulder formation mechanism validated in L-mode to H-mode plasmas with the introduction of a few new elements which will be developed in forthcoming work.

Appendix 1: Acknowledgements

This work has been carried out within the framework of the EUROfusion Consortium and has received funding from the Euratom research and training programme 2014-2018 under grant agreement No 633053. The views and opinions expressed herein do not necessarily reflect those of the European Commission.

Appendix 2: Refences

[1] S. I. Krasheninnikov, Phys. Lett. A 283, 368 (2001).

[2] O. E. Garcia, et al.Plasmas 13, 082309 (2006).

[3] S. I. Krasheninnikov, et al., J. Plasma Phys. 74, 679717 (2008).

[4] J. R. Myra, et al., Phys. Plasmas 13, 092509 (2006).

[5] D. A. Russell, et al., Phys. Plasmas 14, 102307 (2007).

[6] B. LaBombard, et al., Phys. Plasmas 8, 2107 (2001)

[7] D. L. Rudakov, et al., Nucl. Fusion 45, 1589 (2005).

[8] O. E. Garcia, et al., J. Nucl. Mater. 363–365, 575 (2007).

[9] D'Ippolito D.A. and Myra J.R. Phys. Plasmas 13 062503 (2006).

[10] D. Carralero et al., Nucl. Fusion 54 123005 (2014)

[11] J.R. Myra, D. A. Russell and D.A. D'Ippolito, Phys. Plasmas 13 112502 (2006)

[12] D. Carralero et al., J. Nucl. Mater. 123–127, 463 (2015).

[13] R. Panek et al., Plasma Phys. Control. Fusion 58 (2016) 014015.

[14] D. Carralero et al, Phys. Rev. Lett., 115, 215002 (2015)

[15] M. Willensdorfer et al Plasma Phys. Control. Fusion 56 025008 (2014)

[16] C. Theiler, I. Furno, P. Ricci et al., Phys. Rev. Lett. 103, 065001 (2009).

[17] P. Manz, D. Carralero, G. Birkenmeier, et al., Phys. Plasmas 20, 102307 (2013).

[18] B. Nold et al., Plasma Phys. Control. Fusion 52 065005 (2010)

[19] M. Kocan, F. P. Gennrich, A Kendl, et al. Plasma Phys. Control. Fusion 54, 085009 (2012)

[20] D. Carralero, J. Madsen, S. A. Artene, et al., Submitted to Nucl. Mater. Energy (2016)

[21] A. Kallenbach, R. Dux, J. C. Fuchs, et al., Plasma Phys. Control. Fusion, 52, 055002 (2010).

[22] N. Vianello, C. Tsui, C. Theiler, et al., submitted to Fusion Energy Conference (2016)

[23] Lipschultz B., Whyte D. and LaBombard B. Plasma Phys. Control. Fusion 47 1559–78 (2005)